



THE UNIVERSITY *of* EDINBURGH

Edinburgh Research Explorer

Precise Self-Positioning of Colloidal Particles on Liquid Emulsion Droplets

Citation for published version:

Liber, SR, Butenko, AV, Caspi, M, Guttman, S, Schultz, M, Schofield, A, Deutsch, M & Sloutskin, E 2019, 'Precise Self-Positioning of Colloidal Particles on Liquid Emulsion Droplets', *Langmuir*, no. 8. <https://doi.org/10.1021/acs.langmuir.9b01833>

Digital Object Identifier (DOI):

[10.1021/acs.langmuir.9b01833](https://doi.org/10.1021/acs.langmuir.9b01833)

Link:

[Link to publication record in Edinburgh Research Explorer](#)

Document Version:

Peer reviewed version

Published In:

Langmuir

General rights

Copyright for the publications made accessible via the Edinburgh Research Explorer is retained by the author(s) and / or other copyright owners and it is a condition of accessing these publications that users recognise and abide by the legal requirements associated with these rights.

Take down policy

The University of Edinburgh has made every reasonable effort to ensure that Edinburgh Research Explorer content complies with UK legislation. If you believe that the public display of this file breaches copyright please contact openaccess@ed.ac.uk providing details, and we will remove access to the work immediately and investigate your claim.



Precise self-positioning of colloidal particles on liquid emulsion droplets

Shir R. Liber,[†] Alexander V. Butenko,[†] Moshe Caspi,[†] Shani Guttman,[†] Moty
Schultz,[†] Andrew B. Schofield,[‡] Moshe Deutsch,[†] and Eli Sloutskin^{*,†}

*Physics Department and Institute of Nanotechnology & Advanced Materials, Bar-Ilan University,
Ramat-Gan 5290002, Israel, and The School of Physics and Astronomy, University of Edinburgh,
Edinburgh EH9 3FD, UK*

E-mail: eli.sloutskin@biu.ac.il

*To whom correspondence should be addressed

[†]Physics Department and Institute of Nanotechnology & Advanced Materials, Bar-Ilan University, Ramat-Gan
5290002, Israel

[‡]The School of Physics and Astronomy, University of Edinburgh, Edinburgh EH9 3FD, UK

Abstract

Decorating emulsion droplets by particles stabilizes foodstuff and pharmaceuticals. Interfacial particles also influence aerosol formation, thus impacting atmospheric CO₂ exchange. While studies of particles at *disordered* droplet interfaces abound in the literature, such studies for ubiquitous *ordered* interfaces are not available. Here we report such an experimental study, showing that particles residing at crystalline interfaces of liquid droplets spontaneously self-position to specific surface locations, identified as structural topological defects in the crystalline surface monolayer. This monolayer forms at temperature $T = T_s$, leaving the droplet liquid, and driving at $T_d < T_s$ a spontaneous shape-change transition of the droplet from spherical to icosahedral. The particle's surface position remains unchanged in the transition demonstrating these positions to coincide with the vertices of the sphere-inscribed icosahedron. On further cooling, droplet shape-changes to other polyhedra occur, with the particles remaining invariably at the polyhedra's vertices. At still lower temperatures the particles are spontaneously expelled from the droplets. Our results probe the molecular-scale elasticity of quasi-two-dimensional curved crystals, impacting also other fields, such as protein positioning on cell membranes, controlling essential biological functions. Using ligand-decorated particles, and the precise temperature-tunable surface position control found here, may also allow using these droplets for directed supra-droplets self-assembly into larger structures, with a possible post-assembly structure-fixation by UV-polymerization of the droplet's liquid.

Introduction

Micron-size colloidal particles (CPs hereafter), residing at a liquid surface¹, play a central role in microrheology², encapsulation, compartmentalization of synthesis processes, catalysis and emulsification.^{3,4} Surface-residing CPs are also a very simple physical model, reproducing the most fundamental aspects of protein diffusion on a membrane. They are also claimed to mimic a broad range of collective phenomena, ranging from self-assembly of virus capsids and self-organization of magnetic flux vortices in superconductors⁵ to Jeans's gravitational instability in astrophysics.^{6,7}

The remarkable recent progress in the fields above was achieved in studies addressing ordered^{5,8-10} and disordered^{1,2,6,11,12} micron-sized CPs residing at *structureless and disordered* liquid interfaces only. However, many liquid interfaces exhibit some degree of ordering on a molecular scale.¹³⁻¹⁵ In some cases, a disordered liquid bulk coexists, over an extended temperature range, with a crystalline surface monolayer of the same molecules, or a mixed surfactant-alkane Langmuir-Gibbs monolayer.¹⁶⁻¹⁸ CPs embedded in such a planar surface monolayer are essentially immobilized.¹⁹ However, if the crystalline monolayer resides at the surface of a droplet, the spherical topology^{5,9} necessarily dictates the presence of a large number of structural defects within the monolayer²⁰, which should allow a higher mobility, for a single or a few CPs residing at the surface. Thus, fundamentally new dynamics are expected²¹⁻²⁴ to take place for CPs bound at such curved crystalline interfaces. Yet, to our knowledge, no studies of the dynamics of solid particles residing at curved crystalline monolayers are available in the literature.

Here we present such an experimental study of the dynamics of CPs, self-positioned at the curved, ~ 2 nm-thick, crystalline interfacial monolayer of water-suspended liquid oil droplets. Using optical microscopy we demonstrate that the dynamics of these CPs is dominated by the presence of topological defects in the crystalline surface monolayer, over a wide temperature interval below T_s , where the crystalline surface monolayer forms. Furthermore, the droplets studied here were shown to undergo a spontaneous shape transformation^{20,25} where at some $T_d < T_s$ the crystalline surface monolayer reshapes the spherical droplet's surface into a polyhedron with planar facets and vertices (leaving however the droplet's bulk liquid). Here we show that the CPs self-position at these vertices, the aggregation sites of the topological defects of the crystalline surface monolayer.²⁶ Finally, at a still-lower $T_{SE} < T_d$, where the droplets spontaneously emulsify by splitting and by growing long protrusions²⁰, the CPs are expelled from the droplet and remain supported against gravity on the network of the nano-scale protrusions. **We demonstrate the CPs' self-positioning and expulsion to be driven by the elastic energy and the thermodynamics of the crystalline monolayer, covering the surface of these droplets.**

The observed dynamics of CPs in curved two-dimensional (2D) crystals opens the route to-

wards new strategies in self assembly. Ligand-coated CPs, self-positioned at precise locations on the surface of a liquid droplet, allow in principle particle-directed droplets' self-assembly into complex pre-designed clusters, akin to the valence-electron-directed conventional self-assembly of a molecule from its atom constituents. Larger structures, such as promising metamaterials²¹, may be formed as well. Once the relevant structure is formed, the droplets may either be solidified²⁷ or kept liquid. While the present study is just a first step, and much developmental work is still needed, we envision that the ability to dynamically control by temperature-tuning the shape of the droplets, and the presence, properties and location of their surface ligands, could open broad vistas for applications in various fields ranging from directed self-assembly of micromechanical systems (MEMS)²⁸ to targeted delivery and controlled release of medication within the human body.^{29–31}

Background

To better understand our present results on CP-carrying droplets we first recap recent results^{20,25,26} on the temperature evolution of carrier droplets without CPs. These emulsion droplets are water-dispersed *n*-hexadecane droplets (denoted C₁₆) stabilized against coalescence by a cationic surfactant, C₁₈TAB (see Experimental section), having a C₁₈ alkyl tail and a bulky headgroup. The geometry of these molecules promotes their co-crystallization at the droplet's interface.^{18,20,26} In particular, at temperatures $\gtrsim 26^\circ\text{C}$ the droplet's outermost ~ 2 nm-thick monolayer consists of a liquid mixture of C₁₆ and C₁₈TAB molecules, known at planar interfaces as a Langmuir-Gibbs film.^{17,18} The droplet's interfacial tension $\gamma \approx 6$ mN/m dominates the droplet's shape keeping it spherical. Cooling to $T_s \sim 26^\circ\text{C}$, the surface monolayer freezes, forming a hexagonally-packed crystalline monolayer. Further cooling drives the droplets through two consecutive shape transformations: at $T_d < T_s$ spherical droplets facet into icosahedra, and still lower, at $T_{SE} < T_d$, the icosahedra turn into polygonal platelets, which grow elongated protrusions and split into smaller droplets. This sequence is schematically depicted in Figure 1(a). The mechanism of these transformations was lately subject of a significant controversy.^{20,25,32,33} However, recent evidence^{26,27,34} confirms that the transformations are driven by the freezing, at $T_s \approx 26^\circ\text{C}$, of the liquid surface

monolayer into a hexagonally-ordered crystalline monolayer¹⁸, which coexists, unchanged, with the droplet's liquid C₁₆ bulk down to the equilibrium bulk's freezing temperature $T_f \sim 18^\circ\text{C}$. This effect is known as "interfacial freezing". **This effect is different from, and unrelated to, the surfactant multilayers known to adsorb at some specific conditions to the liquid/air surface of different types of surfactant solutions.**³⁵ The interfacial freezing results in a linear decrease in the droplet's interfacial tension γ with decreasing temperature from ~ 6 mN/m above T_s to ~ 0 mN/m at T_{SE} .^{18,20} Thus, although γ is reduced upon cooling below T_s , it is still sufficiently high to dominate the droplet's shape and keep it spherical. At some $T_d < T_s$, however, γ becomes sufficiently low for the elasticity of the crystalline surface monolayer to start dominating the droplet's shape, and a sphere-to-icosahedron shape transition occurs(see Figure 1(a)).

This shape transition occurs because the hexagonal crystalline order of the surface-frozen monolayer is incompatible with a closed, curved surface, such as a spherical droplet's. By Euler's topological theorem^{8,9}, for a hexagonal lattice to perfectly cover such a surface it must have at least 12 defects, i.e. lattice sites with 5, rather than 6, neighbours, as in a soccer ball, where 12 pentagons must be included in the hexagon-tiled outer skin²⁰. These structural defects are known as disclinations, and said to bear a topological charge +1 (6-5=1). Thus, the total topological charge of an hexagonally-ordered crystal covering a closed surface is exactly +12. The elastic energy of a disclination is reduced upon reducing its radius of curvature. Thus, the monolayer buckles spontaneously at T_d outwards from the spherical interface at the disclination points to reduce the local radius of curvature, thus forming the 12 vertices of an icosahedron. The elastic energy is further reduced by the formation of sharp ridges connecting each pair of vertices.^{20,36}

The 12 topology-dictated disclinations are believed to be also at the heart of shape formation in large viruses, bacteriophages, certain radiolaria, and other chemical and biological objects of an icosahedral shape.³⁶⁻³⁸ However, only in the droplets studied here, where the exchange of oil molecules between the interfacial crystal and the droplet's liquid bulk is possible, do the grand-canonical ensemble conditions apply. As a result, the transition sensitively depends on γ , enabling an accurate, and reversible, control of the droplet's shape by tuning its temperature.

The icosahedron-shaped droplets exist over a narrow temperature range only. On cooling below T_d , γ fast reaches zero at T_{SE} , and may even become transiently negative. Since γ is the excess surface free energy per unit area, increasing the surface area for $\gamma < 0$ reduces the system's total free energy. Thus, the icosahedra deform into higher-surface-area shapes, forming hexagonal, triangular, and parallelogram-shaped platelets of finite thickness.²⁷ Some of these shapes exhibit tail-like protrusions, continuously elongating and thinning in this transient regime, to gain surface area. Protrusion formation is quite uncommon for liquid droplets in general. Also, spontaneous droplet splitting events are observed, recently hypothesized to have played a role in division of protocells at the origin of life.³⁹ Finally, the continuously-created surface area increasingly depletes the surfactant's bulk concentration, eventually bringing γ up to zero, at which point the elongation and thinning of droplets and their tails stops.

While the study presented here focuses on a particular model system of C₁₆:C₁₈TAB, many other oil:surfactant combinations have been recently demonstrated to exhibit similar self-faceting phenomena.^{27,40} In some cases, far wider self-faceting temperature ranges have been observed. However, since the present work aims at understanding the fundamental physics of these transitions, we **mainly focus on (arguably) the simplest** and the best-studied of the many chemically-allowed oil:surfactant combinations.

In the following sections we show how the droplet's temperature evolution above, and in particular that of the surface-frozen monolayer, impacts the present observations of the dynamics and positioning of CPs within the droplets, and, at the same time, how these observations further support the faceting and spontaneous emulsification mechanism discussed.

Experimental

To allow focussing on the results, we present here only a brief account of some experimental and computational details. Further details are given in Supplementary Information (SI, Experimental Details).

Samples & Preparation

Three different surfactants, [C18TAB (cationic), SHS (anionic) and Brij-93 (non-ionic)] and two oils, (hexadecane and tetradecane), were used in the experiments. C₁₈TAB (trimethyloctadecylammonium bromide, CH₃(CH₂)₁₇N(CH₃)₃Br, Aldrich, $\geq 99\%$ and $\geq 98\%$ pure) was recrystallized 1-3 times from a methanol - acetone solution. C₁₆ alkane (hexadecane, CH₃(CH₂)₁₄CH₃, Aldrich, 99% pure) and C₁₄ alkane (tetradecane, CH₃(CH₂)₁₂CH₃, Aldrich, $\leq 99\%$) were percolated 2-3 times through fresh activated basic alumina columns to remove polar components. Millipore Ultra-pure 18.2 M Ω ·cm water was used throughout. The hydrophobic PMMA (polymethymethacrylate, stabilized by polyhydroxystearic acid; fluorescently-labeled by DiIC₁₈)⁴¹⁻⁴⁴ and the hydrophobic SicastarTM silica (trimethylsilyl coated) CPs used were spherical and fluorescently-labeled, of diameters $\sim 2.4\ \mu\text{m}$ (PMMA) and 1.5 and 5 – 7 μm (silica). Nanoparticles (trimethylsilyl coated silica, SicastarTM), 250 nm in radius, have been employed as well. To test the sensitivity of the observed phenomena to drastic contact angle variations, we also employed hydrophilic NH₂-coated polystyrene particles (fluorescent MicromerTM, 1.25 μm in radius). Remarkably, no qualitative difference in the behaviour was observed for these very different CP types and sizes. The similar behaviour, in spite of the obviously very different contact angles and contact line pinning properties indicates that these properties do not affect significantly the behaviour reported in this study. The hydrophobic CPs were washed several times with alumina-percolated C₁₆ before use. Brij[®]-93 (Sigma-Aldrich) and SHS (sodium hexadecyl sulfate, CH₃(CH₂)₁₅OSO₃Na, Acros Organics, 99%) were used as received.

For C₁₆:C₁₈TAB emulsion preparation, a 0.5 mM to 1 mM water solution of C₁₈TAB was stirred for ~ 30 minutes at 50°C, ensuring a complete dissolution of the surfactant. Next, 0.8-2% of a dilute suspension of hydrophobic CPs in C₁₆ was added to the surfactant solution and mixed for 2 min, to form an emulsion. The same preparation protocol was also employed for the C₁₆:SHS, C₁₄:SHS, and C₁₆:Brij-93 emulsions; see surfactant concentrations in the SI. The CPs, contained inside the emulsion droplets, settle by gravity to the bottom of the droplets, embedding into the interface. Where hydrophilic CPs were to be loaded onto the surface of the droplets,

we simply added them to the aqueous medium. A fraction of these particles then spontaneously adsorbed to the droplets' surfaces. Samples were contained in $0.1 \times 2 \times 50 \text{ mm}^3$ rectangular sealed glass capillaries, residing in a copper capillary holder, the temperature of which was controlled to $0.01 \text{ }^\circ\text{C}$.

For further details of the sample preparation, microscopy, CP-tracking, and analysis see SI (Experimental Details).

Simulations

For droplet interface elastic energy calculations, we describe the interface by a set of 2562 triangulation vertices, employing the Surface Evolver software.⁴⁵ The edges are Hookean springs, with the stretching energy given by³⁶ $E_s = (\varepsilon/2) \sum_{\langle ij \rangle} (|\mathbf{r}_i - \mathbf{r}_j| - \tilde{a})^2$, where $\varepsilon = \sqrt{3}Y/2$, Y is the 2D Young modulus, \tilde{a} is the unstrained edge's length, and the summation is carried out over all nearest-neighbor vertices. The bending energy is³⁶ $E_d = (\tilde{\kappa}/2) \sum_{\langle IJ \rangle} (\hat{\mathbf{n}}_I - \hat{\mathbf{n}}_J)^2$, where $\tilde{\kappa} = 2\kappa/\sqrt{3}$, κ is the bending modulus, and the summation is over all nearest-neighbor plaquettes of the triangulated surface, with unit normals $\hat{\mathbf{n}}_I$. The bulk volume of the droplet was kept constant, and the dimensionless Föppl-von Kàrmàn number, $\Gamma^{vK} = YR_d^2/\kappa$, was set to $\Gamma^{vK} = 10^3$, consistent with our previous estimates.²⁰ Note, in this range of very large Γ^{vK} the results are not sensitive to its exact value. The equilibrium shape of the interface is found by energy minimization⁴⁵. To estimate the elastic energy gain upon surface adsorption of a CP, we sum the total (bending and stretching) elastic energy associated with the lattice sites enclosed by the CP's three-phase contact line. This energy is, in general, dependent upon the position of the particle's center, as demonstrated in the following by surface energy maps. We note that the present calculation yields only the elastic energy, neglecting any possible entropic and wetting contributions. However, for the experimentally-relevant droplet/CP size ratio, the entropic contributions are expected to be negligible. Also, the fact that particles with completely different interfacial properties exhibit, in our experiments, the same behavior, indicates that the wetting contributions do not play here a significant role.

Results

Main Observations

As a control case for our studies of CP behavior on curved crystals, we first examine the behavior of a single CP inside a droplet at $T > T_s$, where the surface is liquid. In this regime, the particle resides at the bottom of the droplet, as indicated by its position in the center of the droplet's top view in Figure 1(b). Thus, the position of the CP is determined by the gravity, with the CP thermally fluctuating about the droplet's bottom, as demonstrated in Supplementary Movie 1.

This behavior changes drastically upon cooling to $T < T_s$, where the interfacial monolayer is crystalline. As seen in Figure 1(c) and Supplementary Movies 2-3, the CP does not reside at the center of the droplet's top view any more, but is rather shifted away from the center. The new position indicates that the CP is not at the bottom of its gravitational potential well, but rather climbs up on the droplet's spherical interface orders of magnitude higher than achievable by simple thermal agitation.

On further cooling, at $T = T_d$, where γ becomes vanishingly small, and the elasticity of the crystalline surface monolayer drives a sphere-to-icosahedron droplet shape transition (Figure 1(a)), the CP remains at the position it occupied above T_d . This position is now strikingly revealed to be a vertex of the newly-formed icosahedron (Figure 2(a); Supplementary Movie 4). When multiple CPs reside within a droplet, each occupies a different vertex of the faceted droplet, potentially allowing up to 12 CPs to decorate the vertices of an icosahedron (Figure 2(b)).

Further reduction of the temperature, to T_{SE} , transforms the icosahedra into platelet-like polyhedra with fewer vertices. Notably, during a rapid vertex-merging event, a CP may occasionally be pushed away from its vertex. However, it would return to one of the vertices within just a couple of minutes and stay there thereafter. A few examples of such single-CP-decorated platelet-shaped droplets are shown in Figure 2(c-e). Finally, at $T \leq T_{SE}$ we observe catastrophic effects where the flattened droplets exude long, wiry tails, split, and violently expel the CP, all of which destroy the original droplet, dividing up its original oil contents into smaller, independent, entities.

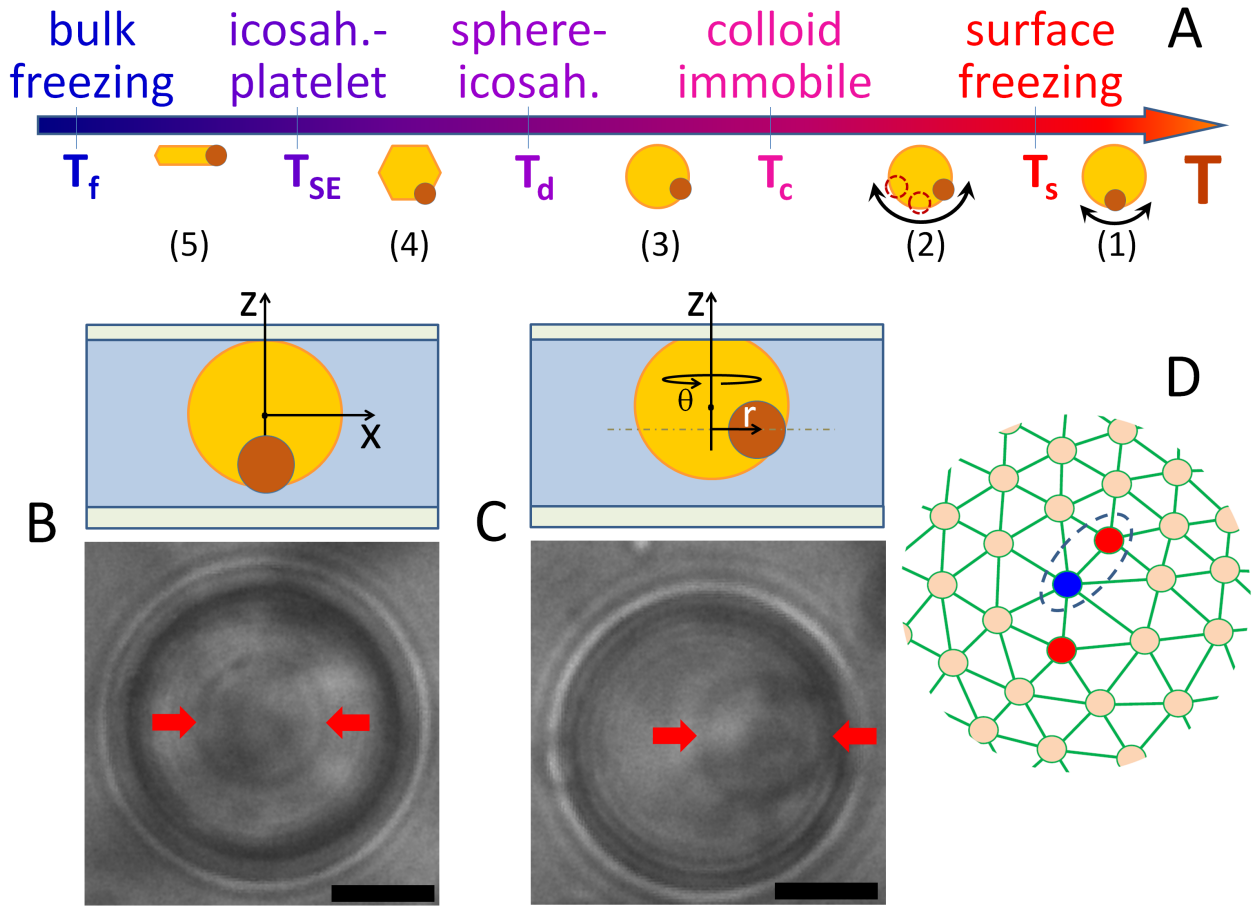


Figure 1: Experimental geometry and optical microscopy images of a CP residing at a droplet's surface. (a) Temperature sequence of the various transitions in the phase and shape of the droplet (yellow), and in the dynamics and position of the particle (brown), numbered in the order they occur upon cooling. See temperature values in Table 1 (SI). (b-c, Top) An oil droplet, suspended in an aqueous surfactant solution (light blue). CPs reside at the droplet's surface. (b-c, Bottom) Droplet micrographs (imaged from below). The CP is marked by arrows. The droplet's center-of-mass Cartesian (b) and cylindrical (c) coordinate systems are shown. (b) When the droplet's interface is liquid ($T > T_s$), the CP resides at the droplet's bottom. (c) When the interface is crystalline ($T < T_s$), the particle climbs up and self-locates onto one of the 12 topology-dictated disclinations. The imaging plane is marked by a dash-dotted line in (c); note also the minute buoyancy-induced flattening of the droplet's top in this cartoon. Scale bars are $5 \mu\text{m}$. The temperature values are provided in the SI (Table 2). (d) A balanced pair of disclinations, (lattice sites with coordination numbers smaller (red) and larger (blue) than 6) forming a dislocation, is encircled by dashes, near an unbalanced disclination (red).

To confirm the generality of the observed phenomena, we repeated the experiments with a wide range of particle sizes, of radii varying by more than an order of magnitude, from 250 nm to 3.5 μm . We have also experimentally confirmed that similar effects take place for both the hydrophobic (Supplementary Movies 1-4) and the hydrophilic (Supplementary Movie 5) colloids, demonstrating no significant dependence on either the contact angle of the liquid with the particle or the specific surface chemistry. Since the contact line pinning effects are, in general, sensitive to the chemistry and the roughness of the surface², the role of these effects in the observed phenomena is insignificant.

To clarify the mechanism of the discovered phenomena, we probed the droplet's interface by following the dynamics of an individual particle residing at the interface. Remarkably, while the interfacial freezing dramatically slows down the thermal motion of the particles at $T < T_s$, the motion is not completely arrested. This behavior contrasts with the complete arrest of particles residing at a *planar* interface, at $T < T_s$ (see Section 2 in the SI). The higher mobility of particles embedded in a curved crystalline monolayer suggests that this crystal is less perfectly ordered than a planar one. Indeed, in addition to the 12 disclinations of topological charge +1, dictated for a curved crystal by Euler's theorem^{8,9}, such crystals also typically develop additional lattice defects to alleviate the stress imposed by the curvature.⁹ These additional defects appear in pairs: a five-coordinated lattice site is accompanied by a seven-coordinated one, i.e. a -1 -charge disclination, balancing the pair (Figure 1(d)). Such a pair, called a 'dislocation', carries no net topological charge, so that the total topological charge for an hexagonally-packed crystal wrapping a closed surface remains exactly 12. While planar interfacial crystalline monolayers exhibit mm-size single-crystal domains¹⁶, spherical crystalline monolayers possess high defect concentrations, even in their ground state. We suggest that these higher defect concentrations are responsible for the higher particle mobilities at $T < T_s$.

Furthermore, we suggest that the topological defects are also responsible for the CPs' self-positioning. In particular, owing to the topological defects, the lattice stress distribution in spherical crystals breaks the rotational symmetry: the in-plane stress peaks at each of the 12 unbal-

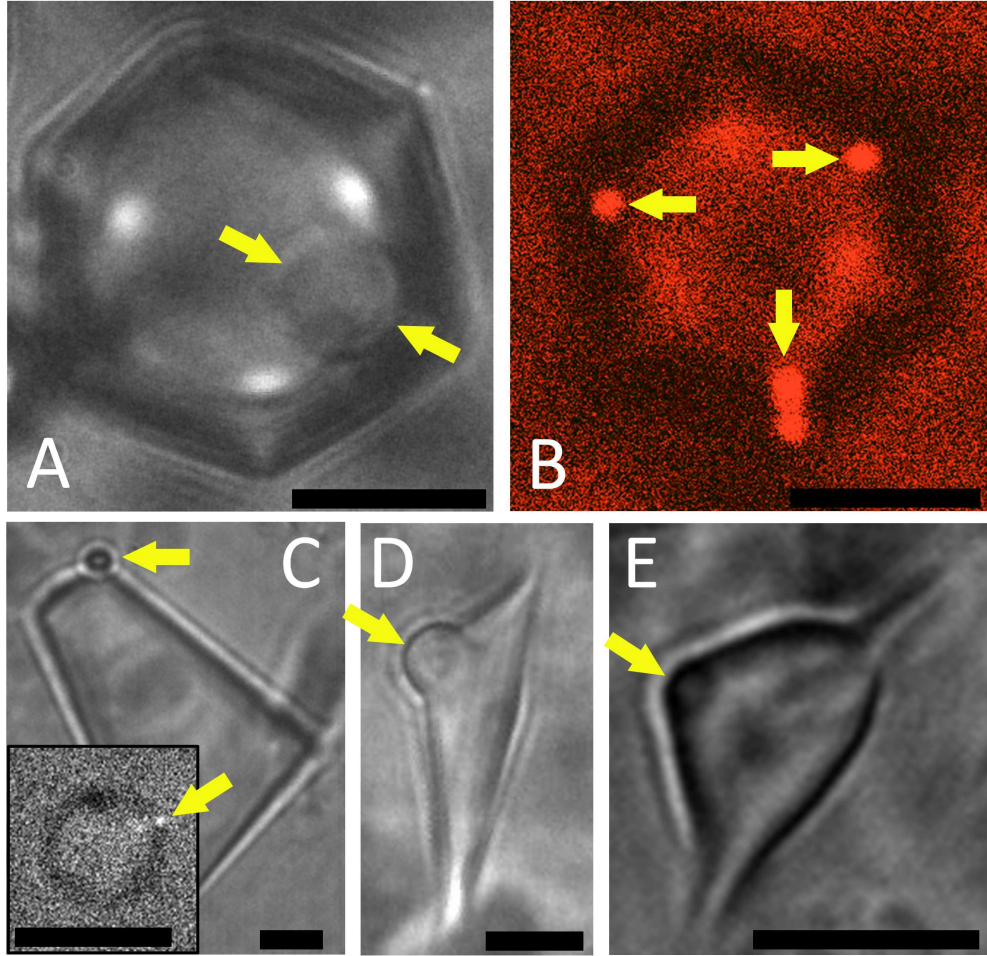


Figure 2: CPs' self-positioning at the vertices of the faceted liquid oil droplets. Note the generality of the effect for CP radii ranging from $0.25 \mu\text{m}$ (inset to (c)) to $3.5 \mu\text{m}$ (a). (a) An individual CP sitting at the vertex of an icosahedron-shape liquid droplet ($T_{SE} < T < T_d$) is marked by yellow arrows. The positions of the 3 bottom vertices of the icosahedron are roughly half-way between the bright white spots, corresponding to the topmost vertices. (b) Three fluorescent CPs, spontaneously adopting the 3 bottom vertex locations of an icosahedron, are marked by arrows. One of the CPs has a shape of a dumbbell, formed by an irreversible adhesion of two colloidal spheres. Here the diameter of the CPs is $\sigma \approx 1.5 \mu\text{m}$; the droplet's diameter is $19.4 \mu\text{m}$. (c) A CP spontaneously attached to one of the vertices of a platelet-like faceted droplet at $T \lesssim T_{SE}$. The inset shows a much smaller particle (marked by an arrow), only 250 nm in radius, spontaneously self-positioned onto one of the vertices of an icosahedral droplet. Even smaller particles may be exhibiting the same phenomena as well; yet, the imaging of such small particles on non-fluorescent droplets is highly challenging. (d-e) CPs self-positioned at vertices of complex-shape droplets at $T \lesssim T_{SE}$. All scale bars are $10 \mu\text{m}$. The temperature values are provided in the SI (Table 2).

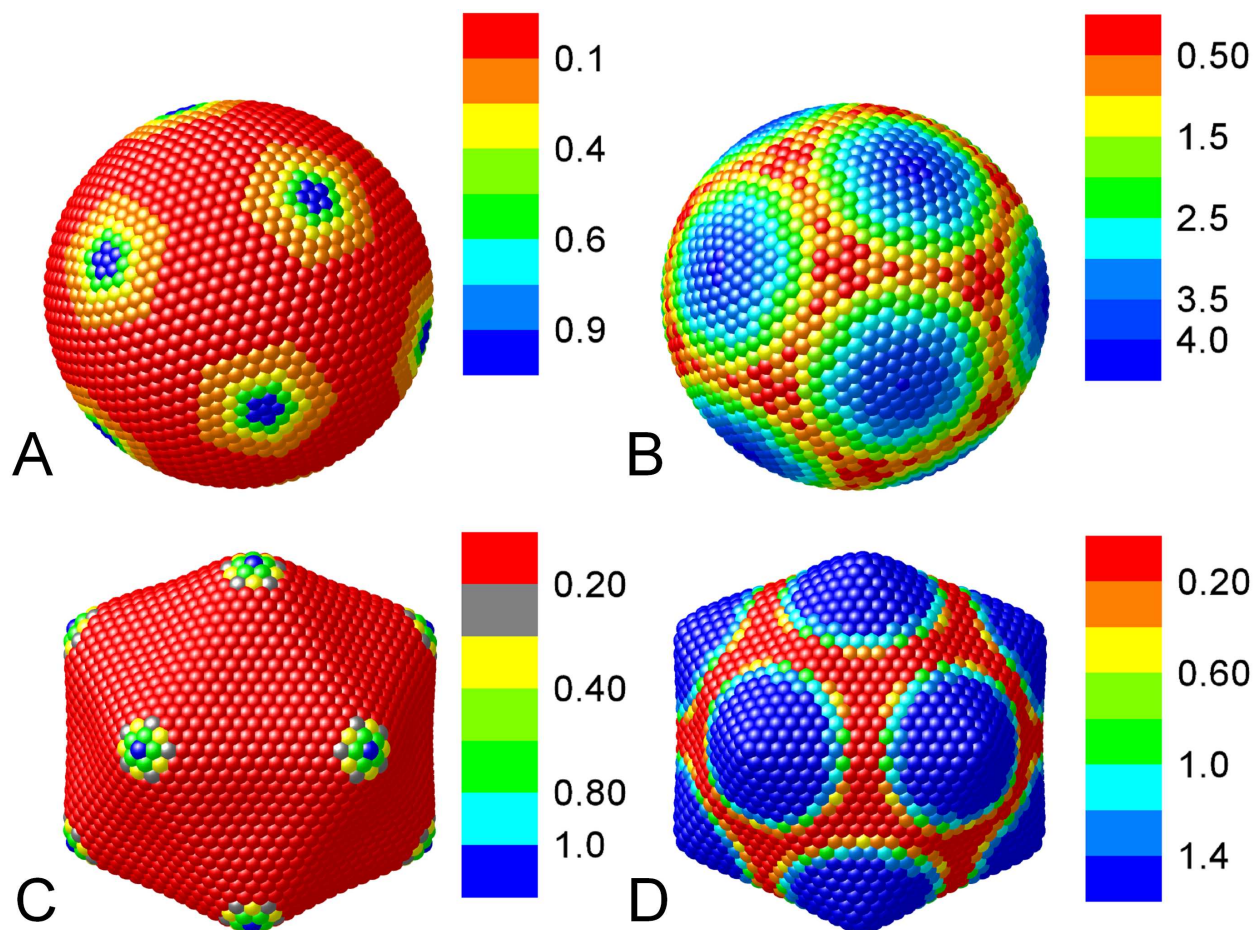


Figure 3: The elastic energy gain (see color map) on piercing the interfacial crystalline monolayer of a R_d -radius droplet by an adsorption of a colloidal particle. The contact line of the piercing particle is assumed to be an ideal circle of radius a_c . The a_c/R_d ratio was chosen as either 0.08 ((a) and (c)) or 0.5 ((b) and (d)), within our present experimental range. The energy values in the color map labels were divided by $(\sqrt{3}/2000)YR_d^2$, to render values non-dimensional. Y is the 2D Young modulus. Note the significantly larger energy gain at the 12 disclination locations, with the droplet adopting either a spherical ($T_d < T < T_s$, (a)-(b)) or an icosahedral ($T_{SE} < T < T_d$, (c)-(d)) shape.

anced disclinations.⁴⁶ Thus, the energy gain on piercing the interfacially-frozen monolayer by a CP and thus eliminating some high-extensional-energy surface area, strongly depends on the point of piercing. The energy gain is higher when the center of the CP coincides with the disclination core, as shown in the calculated elastic energy gain in Figure 3(a-b). With the Y value previously²⁰ estimated as $6 \times 10^{-4} < Y < 0.04$ N/m, the calculated elastic attraction energies of our particles towards the disclinations are above $10^4 k_B T$, far exceeding their (buoyancy-subtracted) gravitational energy and any entropy-driven position randomization, being only a few $k_B T$ effect. Consequently, upon formation of the crystalline monolayer (and hence the disclinations) at $T = T_s$, the CPs are strongly attracted to the disclinations. Defying gravity they climb up on the droplet's surface and self-position at a disclination to reduce the system's elastic energy, as observed in Figure 1(c). A similar particle attraction to disclination cores in three-dimensional liquid crystals was demonstrated to drive self-assembly of colloidal structures.^{47,48} Also, particle attraction to defects in thick⁴⁹ nematic shells⁵⁰ and nematic-defect-controlled phase-separation in molecular monolayers⁵¹ have been studied. Yet, no particle-defect attractions have been studied for curved *crystals*, and particularly for the two-dimensional ones. Note that our present calculations (Figure 3) account only for the elastic energy of particle positioning on the surface and do not provide any dynamical information. More advanced simulations, potentially allowing to reproduce the full dynamics of our particles' *en-route* to the disclinations, are clearly indicated.

In this $T < T_s$ regime, where the droplet's surface is covered by a two-dimensional crystal, the particle trajectory (shown in Figure 4(b)) is much more extended in length than the compact well-centered trajectories at $T > T_s$ (Figure 4(a)). Remarkably, the particle spends longer times at certain locations, then rapidly moves to a new place, as seen in the stair-like time-dependence of its Cartesian x -coordinate (Figure 4(e)). We propose that each $x(t)$ -plateau in this plot corresponds to the particle being transiently trapped at a specific disclination. For comparison we show in Figure 4(d) the corresponding $x(t)$ at $T > T_s$, where the interfacial layer is liquid: only random fluctuations are observed around $x = 0$, the position of the droplet's bottom (see also Supplementary Movies 1 and 2).

Surprisingly, at a slightly lower temperature $T_c < T_s$, but still above the faceting transition temperature (see Figure 1(a)), the trajectory changes again and becomes compact, as for $T > T_s$. However, the CP is now even more strongly shifted away from the bottom of the droplet (Figure 4(c); Supplementary Movie 3). Moreover, the CP's motion is now almost completely arrested (SI, Section 2). The sudden arrest of the CP's mobility suggests that it is now fixed at one of the disclinations. To verify this assumption, note that same-sign topological charges repel each other, as do electrostatic charges, with the repulsion being mediated by the stresses in the 2D crystalline lattice. Thus, in a crystalline monolayer wrapping a sphere, the unbalanced disclinations should be located at the vertices of an inscribed icosahedron, since these positions maximize their distances from each other (see Figure S2 in the SI). On cooling below T_s , the interfacial tension reduces dramatically, so that the top of the droplet is slightly flattened by buoyancy against the top wall of the capillary (Figure 1(c)).²⁶ This effect, used in our previous work to quantitatively estimate the value of γ *in situ* for much larger droplets²⁶, does not allow the droplet to rotate while the colloidal particle climbs up on its wall. Moreover, the flattening at the droplet's top slightly reduces the local radius of curvature next to the flattened region. Such higher-curvature regions are known to attract the disclinations⁴⁶; thus, the total energy of the 12 canonical disclinations is reduced if 3 of them are located around the boundary of the flattened top region of the droplet. In Section 3 of the SI, we use these facts to calculate the expected disclination-bound CP positions on a spherical droplet, with the results further supporting our conclusions.

Note that while particle attraction to high-curvature regions of liquid interfaces is well-known⁵², this effect is negligible in our case, since the buoyancy-induced distortions of these droplets only occur at very low γ . The energy of particle attraction towards a region of high (mean or deviatoric) curvature⁵² increases monotonically with γ . This increase takes place in spite of the concomitant weakening of droplet shape distortions. As no evidence for high-curvature attraction is observed for our droplet sizes at $T > T_s$ ($\gamma \approx 6$ mN/m), the effect must be completely negligible at $T < T_s$, where γ is much lower (down to ~ 0.1 mN/m at T_d). **Thus, we conclude that the CPs' self-positioning is driven by the elasticity of the interfacially-frozen crystal, as described above.**

Finally, additional measurements are needed to establish whether the crossover to the low-mobility regime at T_c (Figure 4(c,f)) is purely temperature-driven, with a true phase transition occurring at that temperature. Currently, we cannot exclude a different scenario for the trajectory compaction, where the sudden interfacial freezing at T_s creates redundant grain boundaries in the crystalline surface monolayer. As these heal with time, the CP motion is increasingly restricted to the regions of the 12 topologically-dictated disclinations and perhaps a few energetically-favorable dislocation ‘scars’.⁹

Particle Positions on the Icosahedra.

To further test our guess that the CPs are sitting at the disclinations, we cool below T_d , where the spherical liquid droplet shape-transforms into a liquid icosahedron. With this transition, the in-plane stress of the disclinations is partly relieved by the increase of the local curvature. Remarkably, a very modest fine-tuning of the position of the CP suffices to place it at the vertex of the icosahedron formed. Thus, we conclude that the CP was located close to one of the disclinations already above T_d , where the droplet was still spherical. A previous theoretical study predicted segregation of impurities to the topological defects of a spherical nematic **surface**, proposing that this phenomenon may be employed to decorate a spherical colloidal particle with ligands.²¹ However, remarkably, in that theoretical study, as also in a related experimental work⁵¹, the shape of the spherical surface was fixed and the buckling into an icosahedral shape was not allowed. More recent theoretical²² and experimental^{23,24} studies of curved crystal interstitials are also subject to the same restriction. These studies demonstrated the interstitials to fractionate into dislocations, which were then attracted to the neighboring disclinations. The role of an unbalanced disclination as an attractor of defects and impurities is common to our work and these previous studies. However, note that our CPs are more than 3 orders of magnitude larger than the lattice constant of the underlying crystalline monolayer, and therefore can not be considered to be interstitials. Also, the faceting transition, not considered in these previous studies, partly relaxes the lattice stress associated with the disclinations, thus reducing their tendency to attract impurities. Remarkably, in spite

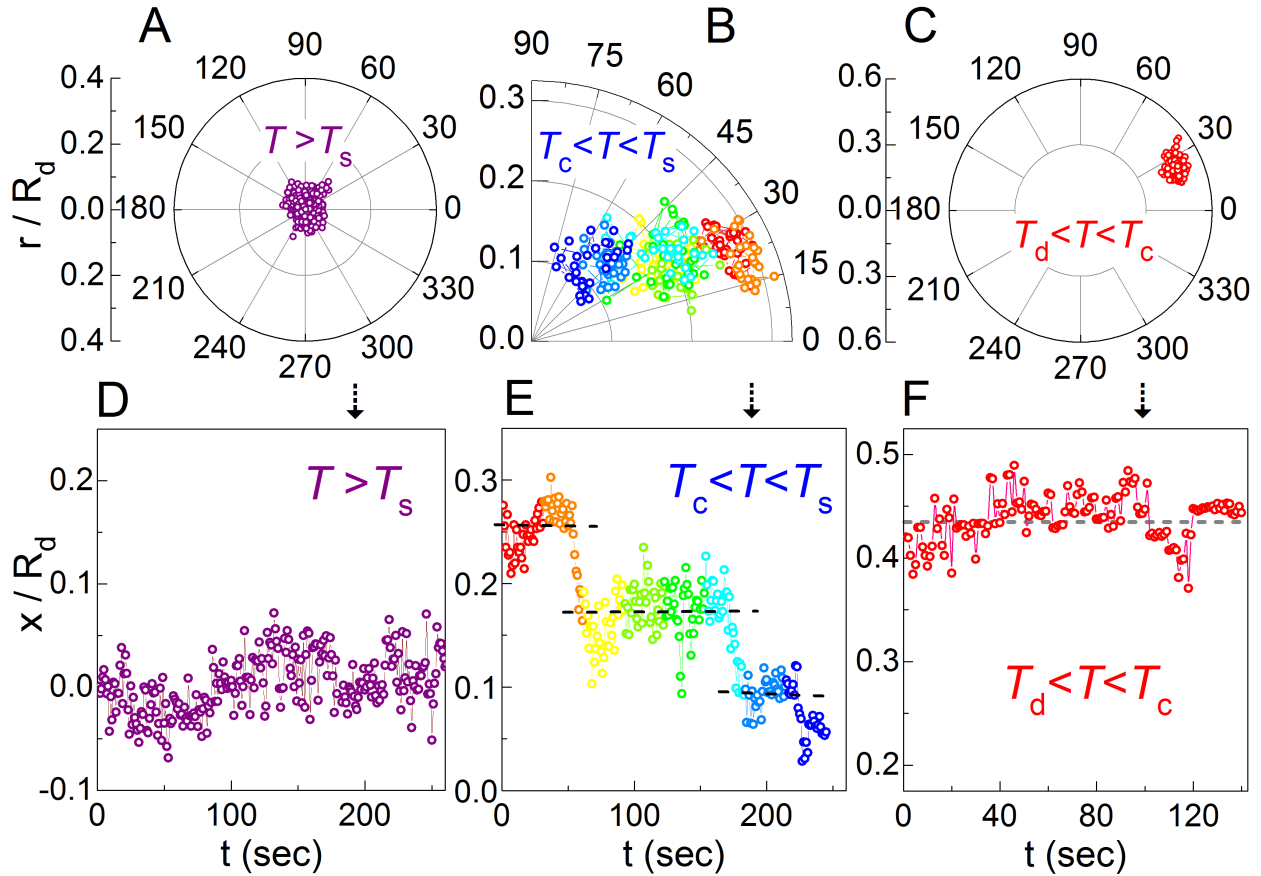


Figure 4: Measured CP trajectories (a)-(c) on spherical liquid droplets in different T -regimes. The corresponding $x(t)$ displacement data are shown in (d)-(f). (a) When the surface is liquid ($T > T_s$) the CP diffuses thermally at the droplet's bottom. Its thermal energy only suffices for climbing a few nanometers against Earth's gravity. (b) At $T_c < T < T_s$, the surface is a crystalline monolayer, and the CP does not follow conventional diffusion but is rather dominated by the complex non-equilibrium distribution of transient defects within the spherical interfacial crystalline monolayer. The time is indicated by different colors, emphasizing the hopping motion observed for this trajectory; note the three positions where the particle stays the longest. These positions are marked by dashed lines in the corresponding $x(t)$, shown in (e). (c) At $T_d < T < T_c < T_s$ (see Figure 1(a)), the surface is crystalline and all transient defects healed. The CP is immobilized at one of the disclinations, exhibiting only slight vibrations about its mean position. The droplet and (hydrophobic) CP radii are $\approx 7.5 \mu\text{m}$ and $\approx 3.5 \mu\text{m}$, respectively. The temperatures are provided in the SI (Table 2).

of this fact, the CPs are clearly observed to self-position at the disclinations of the droplets studied here, even when the droplets are faceted. The presence of particle-disclination attractions is further supported by our elastic energy calculations [Figure 3(c-d)] **indicating that the magnitude of this effect exceeds by several orders of magnitude the CPs' translational entropy contributions to the free energy, which are of the order of $\sim 1 k_B T$, as compared to the order of $10^4 k_B T$ extensional elastic energies in Figure 3. Thus, the CP-disclination attractions, driven by the elasticity of the interfacially-frozen crystalline monolayer, are sufficiently strong to immobilize the particles at the vertices of the liquid icosahedra.**

As the curvature at the vertex tips of the liquid icosahedra is very high, **an additional contribution due to** the capillary attraction of CPs by the curvature⁵² cannot be excluded, in spite of the very low $\gamma \leq 0.1$ mN/m in this regime.^{20,26} To the best of our knowledge, none of the existing theoretical models of capillary attraction is applicable to our situation, where the curvature of the liquid interface at the defect core far exceeds the surface curvature of the solid CP itself. The theoretical treatment of such extreme curvatures, occurring in the rather-unusual ultralow γ regime, is clearly called for.

Particle Expulsion from Platelet-like Droplets.

To test for the particle-vertex attractions at even lower $\gamma \leq 0$, where no capillary attractions should exist, we cool the system to $T = T_{SE}$. Upon collapse of the icosahedral droplets at $T = T_{SE}$, some of the 12 unbalanced disclinations merge. The vertices of the collapsed platelet-like droplets are sharper, with their smaller radii of curvature stabilizing their higher topological charges.²⁶ Such lattice sites with coordination numbers smaller than 5 are rarely encountered in soft matter. Occasionally, the shape transitions are too fast for the CPs to follow the vertices' repositioning in real time; yet, given time, the CPs eventually self-position onto the newly-formed vertices, clearly demonstrating that the CP-disclination attraction is significant, in spite of the ultralow or even transiently negative γ values in this regime²⁶ (see Supplementary Movies 6 and 7).

The ultralow or transiently-negative γ at $T < T_{SE}$ dramatically decrease the interface affinity

of the CPs. This is demonstrated by the CPs' detachment from the interface especially where a mechanical perturbation of the surface is caused by a spontaneous droplet splitting event. On detachment, the CPs, even the hydrophobic ones, are expelled from the oil droplets into the aqueous phase (Supplementary Movies 5-9). However, in spite of their mass density significantly exceeding the water's, they do not sediment to the bottom of the capillary. Rather, their sedimentation is blocked by the dense network of hydrophobic nano-scale tails formed by the neighboring emulsion droplets (Supplementary Movie 6). The exact nature of the attachment of these CPs to the network is yet unclear, due to the optical resolution limit of the microscope. Future research, employing either super-resolution optical microscopy or electron microscopy, should allow resolving whether the CPs are fully enclosed within a single nano-tail, the cross-section of which is dramatically inflated at the particle location. Alternatively, the hydrophobic particle may be physically entangled inside the complex network of nano-tails, with its surface possibly hydrophilized by the C₁₈TAB surfactant adsorption.^{53,54}

Generality of the observed phenomena

To demonstrate that the observed phenomena are general for the faceted liquid droplets and do not depend on the particular chemistry of the system, we replace the cationic C₁₈TAB surfactant by the anionic surfactant SHS. The alkyl tail length and the head group cross section of the SHS are slightly smaller than those of the C₁₈TAB. Yet, the emulsion droplets of C₁₆, suspended in an aqueous SHS solution (3 mM), undergo the sphere-to-icosahedron transition at an even higher $T_d \approx 29^\circ\text{C}$. As for the C₁₈TAB-stabilized emulsions, CPs adsorbed to the droplets' interfaces, spontaneously self-position to the vertices of the icosahedral droplets (Figure 5(a)). On further cooling, the SHS-stabilized droplets undergo an icosahedron-to-platelet transition, with the particles first residing at the droplets' vertices (Figure 5(b)) and then being expelled from the droplets (Supplementary Movie 9). The fact that the behavior is identical for both the cationic (C₁₈TAB) and the anionic (SHS) surfactant, strongly supports the elasticity-based mechanism of the particle

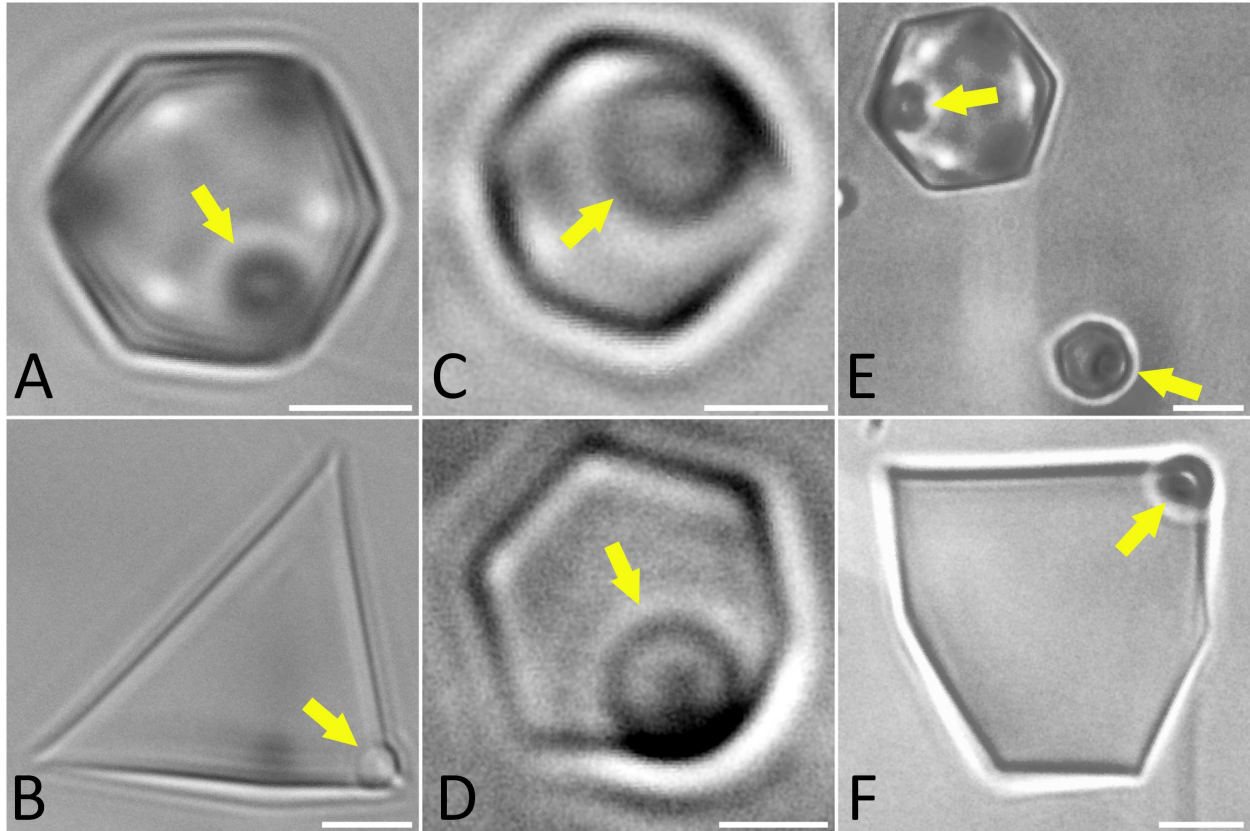


Figure 5: PMMA CPs, self-positioned at the vertices of faceted, SHS-stabilized (a-b) and Brij[®]-93-stabilized (c-d) C₁₆ droplets, demonstrate that the self-positioning phenomenon is independent of the surfactant being either cationic (C₁₈TAB), anionic (SHS), or non-ionic (Brij[®]-93). Moreover, this phenomenon is not restricted to the C₁₆ oil, as demonstrated by particle self-positioning on SHS-stabilized droplets of the C₁₄ alkane (e-f). The CPs are marked by the yellow arrows. The droplet shapes are icosahedral in (a), (c) and (e), where $T_{SE} < T < T_d$; the droplets are platelet-like in (b), (d) and (f), where $T \lesssim T_{SE}$. In the icosahedral droplets, the CP is located at one of the 3 bottom vertices, as in Figure 2(a). The temperatures are: 26, 25, 11.3, 11.0, 24.5 and 19.7°C in (a),(b),(c), (d), (e) and (f), respectively. The scale bar lengths are 5 μm in (a-b, e-f) and 2 μm in (c-d).

self-positioning, described above.

Moreover, we completely rule out the possibility that the self-faceting of the droplets and/or the self-positioning of the CPs are driven by the electrostatic repulsions between the ionized surfactant head groups.^{38,55,56} For that, we employ the same hexadecane-in-water emulsion, but this time stabilized by a non-ionic Brij[®]-93 surfactant (1.5% w/w). Remarkably, we still observe the particles' self-positioning at the vertices of the liquid droplets, exactly as in presence of the ionic surfactants (see Figure 5(c) and (d), for an icosahedral and a platelet-like Brij[®]-93-stabilized droplet, respectively). These observations emphasize that the particles' self-positioning is driven by the topology-dictated elastic effects, due to the 2D crystalline interfacial monolayer. The particular chemistry of the surfactant does not matter, as long as the interfacial-freezing effect occurs in this system.

To further check the generality of the self-positioning effects discussed here, we also examined CPs positioning in a SHS-stabilized tetradecane-in-water emulsion. As demonstrated in Figure 5(e-f), the same positioning effects are observed. While it is not possible to test all numerous emulsion droplet systems exhibiting faceting^{27,40}, our present observations clearly suggest that the self-positioning phenomena are a general feature of all interfacially-frozen emulsions.

As the present studies are limited by the resolution of the optical microscopy, CPs' self-positioning on droplets smaller than $R_d \approx 1.5 \mu\text{m}$ cannot be clearly resolved. Yet, our recent cryo electron microscopy studies indicate that the faceting phenomenon is exhibited by even much smaller droplets, less than a zeptoliter in volume.³⁴ The physical mechanism driving the faceting of these nanodroplets is the same as in our present studies: the elasticity of the interfacially-frozen crystalline monolayer. The bending modulus of the nanodroplets' interfacial crystals is much lower, possibly due to the extreme curvature of the interface in these droplets. However, the CPs' self-positioning is mainly driven by the extensional Y modulus, which does not seem to vary significantly³⁴ with R_d . Future studies, employing electron microscopy, may possibly reveal the bottom limit on R_d , below which no (nano)particles self-positioning takes place.

Conclusion

The observed self-positioning of colloidal particles onto specific locations of a spherical crystalline monolayer, and their anomalous dynamics, demonstrate the unusual physics of the curved crystals, where defects are dictated by topological constraints, present even in the crystal's ground state. Furthermore, the ability to account for all experimental observations in the different temperature regimes by the presence and properties of a surface-frozen crystalline monolayer in coexistence with the droplet's liquid bulk, further supports our interpretation that the observed faceting and self-emulsification transitions in these droplets are controlled by the elasticity of the crystalline monolayer.²⁰

The behaviour found **and accounted for theoretically** here will also prevail in other systems exhibiting interfacial crystallization of the outermost monolayer, such as other alkane/surfactant combinations.^{18,20} Moreover, the universal nature of the interplay between curvature and 2D crystallinity suggests that the behavior uncovered here should be relevant well beyond the class of systems studied here. Partial, or full, surface ordering occur, e.g., also in liquid crystals, ionic liquids, liquid metals and alloys, and alkyl-side-chain polymer droplets. Also, lipid membranes exhibit some degree of hexagonal order and were suggested to include separate crystalline domains.⁵⁷ Topological defects, created by the interplay between the curvature of the lipid membranes and their interface-parallel structure, may play an important role in precise positioning of membrane proteins⁵⁸ and in the control of essential biological processes.⁵⁹ The mechanisms found here for precise droplet surface decoration by solid particles may be used in the future to organize membrane protein molecules on flexible surfaces, allowing the impact of interfacial structure and curvature on their properties to be studied in much simpler physical settings and providing a new strategy towards the assembly of fully-functional artificial "living" cells. Finally, this study emphasizes the need for a full quantitative theoretical treatment of faceting in liquid emulsion droplets as well as of the CP behaviour at their surfaces, presented in this study.

Supporting Information

Supplementary text, Figures S1-S3 and Tables 1-2, providing the technical details of sample preparation, experimental methods, computer simulation techniques, control measurements and particle characterization, particle dynamics data, and particle positioning geometry; Supplementary Movies 1-9 and their captions, demonstrating the on-droplet dynamics of CPs, for both the hydrophobic and the hydrophilic particles, with different surfactants, and for both individual and multiple CPs residing on a droplet.

Acknowledgement

We thank S. Rubinstein, L. Giomi, and I. Garcia-Aguilar for discussions, and J. Feigel - for technical assistance. This research is supported by the Israel Science Foundation (Grant No. 1779/17). We thank Kahn foundation for funding of the equipment.

References

- (1) Kaz, D. M.; McGorty, R.; Mani, M.; Brenner, M. P.; Manoharan, V. N. Physical ageing of the contact line on colloidal particles at liquid interfaces. *Nat. Mater.* **2011**, *11*, 138–142.
- (2) Boniello, G.; Blanc, C.; Fedorenko, D.; Medfai, M.; Ben Mbarek, N.; In, M.; Gross, M.; Stocco, A.; Nobili, M. Brownian diffusion of a partially wetted colloid. *Nat. Mater.* **2015**, *14*, 908–912.
- (3) Yang, H.; Fu, L.; Wei, L.; Liang, J.; Binks, B. P. Compartmentalization of incompatible reagents within Pickering emulsion droplets for one-pot cascade reactions. *J. Am. Chem. Soc.* **2015**, *137*, 1362–1371.
- (4) Butt, H.-J. *Particle-stabilized emulsions and colloids: formation and applications*; Royal Society of Chemistry: Cambridge, UK, 2014.

- (5) Guerra, R. E.; Kelleher, C. P.; Hollingsworth, A. D.; Chaikin, P. M. Freezing on a sphere. *Nature* **2018**, *554*, 346–350.
- (6) Bleibel, J.; Dominguez, A.; Oettel, M. Colloidal particles at fluid interfaces: Effective interactions, dynamics and a gravitation - like instability. *Eur. Phys. J. Spec. Top.* **2013**, *222*, 3071–3087.
- (7) Bleibel, J.; Dietrich, S.; Domínguez, A.; Oettel, M. Shock Waves in Capillary Collapse of Colloids: A Model System for Two-Dimensional Screened Newtonian Gravity. *Phys. Rev. Lett.* **2011**, *107*, 128302.
- (8) Meng, G.; Paulose, J.; Nelson, D. R.; Manoharan, V. N. Elastic Instability of a Crystal Growing on a Curved Surface. *Science* **2014**, *343*, 634–637.
- (9) Bausch, A.; Bowick, M.; Cacciuto, A.; Dinsmore, A.; Hsu, M.; Nelson, D.; Nikolaidis, M.; Traveset, A.; Weitz, D. Grain boundary scars and spherical crystallography. *Science* **2003**, *299*, 1716–1718.
- (10) Nikolaidis, M. G.; Bausch, A. R.; Hsu, M. F.; Dinsmore, A. D.; Brenner, M. P.; Gay, C.; Weitz, D. A. Electric-field-induced capillary attraction between like-charged particles at liquid interfaces. *Nature* **2002**, *420*, 299–301.
- (11) Danov, K. D.; Kralchevsky, P. A.; Boneva, M. P. Electrodippling force acting on solid particles at a fluid interface. *Langmuir* **2004**, *20*, 6139–6151.
- (12) Fuller, G. G.; Vermant, J. Complex fluid-fluid interfaces: rheology and structure. *Annu. Rev. Chem. Biomol. Eng.* **2012**, *3*, 519–543.
- (13) Haddad, J.; Pontoni, D.; Murphy, B. M.; Festersen, S.; Runge, B.; Magnussen, O. M.; Steinrück, H.-G.; Reichert, H.; Ocko, B. M.; Deutsch, M. Surface structure evolution in a homologous series of ionic liquids. *Proc. Natl. Acad. Sci. U.S.A.* **2018**, *115*, E1100–E1107.

- (14) Ocko, B. M.; Braslau, A.; Pershan, P. S.; Als-Nielsen, J.; Deutsch, M. Quantized Layer Growth at Liquid-Crystal Surfaces. *Phys. Rev. Lett.* **1986**, *57*, 94–97.
- (15) Chattopadhyay, S.; Uysal, A.; Stripe, B.; Evmenenko, G.; Ehrlich, S.; Karapetrova, E. A.; Dutta, P. Structural Signal of a Dynamic Glass Transition. *Phys. Rev. Lett.* **2009**, *103*, 175701.
- (16) Ocko, B. M.; Wu, X. Z.; Sirota, E. B.; Sinha, S. K.; Gang, O.; Deutsch, M. Surface Freezing in Chain Molecules: Normal Alkanes. *Phys. Rev. E* **1997**, *55*, 3164–3182.
- (17) Sloutskin, E.; Sapir, Z.; Bain, C. D.; Lei, Q.; Wilkinson, K. M.; Tamam, L.; Deutsch, M.; Ocko, B. M. Wetting, mixing, and phase transitions in Langmuir-Gibbs films. *Phys. Rev. Lett.* **2007**, *99*, 136102.
- (18) Tamam, L.; Pontoni, D.; Sapir, Z.; Yefet, S.; Sloutskin, E.; Ocko, B. M.; Reichert, H.; Deutsch, M. Modification of deeply buried hydrophobic interfaces by ionic surfactants. *Proc. Natl. Acad. Sci. U.S.A.* **2011**, *108*, 5522–5525.
- (19) Bonales, L. J.; Ritacco, H.; Rubio, J. E. F.; Rubio, R. G.; Monroy, F.; Ortega, F. Dynamics of ultrathin films: particle tracking microrheology of Langmuir monolayers. *Op. Phys. Chem. J.* **2007**, *1*, 25–32.
- (20) Guttman, S.; Sapir, Z.; Schultz, M.; Butenko, A. V.; Ocko, B. M.; Deutsch, M.; Sloutskin, E. How faceted liquid droplets grow tails. *Proc. Natl. Acad. Sci. U.S.A.* **2016**, *113*, 493–496.
- (21) Nelson, D. R. Toward a tetravalent chemistry of colloids. *Nano Lett.* **2002**, *2*, 1125–1129.
- (22) Bowick, M. J.; Nelson, D. R.; Shin, H. Interstitial fractionalization and spherical crystallography. *Phys. Chem. Chem. Phys.* **2007**, *9*, 6304–6312.
- (23) Irvine, W. T. M.; Bowick, M. J.; Chaikin, P. M. Fractionalization of interstitials in curved colloidal crystals. *Nat. Mater.* **2012**, *11*, 948–951.
- (24) Soni, V.; Gómez, L. R.; Irvine, W. T. M. Emergent geometry of inhomogeneous planar crystals. *Phys. Rev. X* **2018**, *8*, 011039.

- (25) Denkov, N.; Tcholakova, S.; Lesov, I.; Cholakova, D.; Smoukov, S. K. Self-shaping of oil droplets via the formation of intermediate rotator phases upon cooling. *Nature* **2015**, *528*, 392–395.
- (26) Guttman, S.; Sapir, Z.; Ocko, B. M.; Deutsch, M.; Sloutskin, E. Temperature-tuned faceting and shape-changes in liquid alkane droplets. *Langmuir* **2017**, *33*, 1305–1314.
- (27) Marin, O.; Alesker, M.; Guttman, S.; Gershinsky, G.; Edri, E.; Shpaisman, H.; Guerra, R. E.; Zitoun, D.; Deutsch, M.; Sloutskin, E. Self-faceting of emulsion droplets as a route to solid icosahedra and other polyhedra. *J. Colloid Interf. Sci.* **2019**, *538*, 541–545.
- (28) Syms, R. R. A.; Yeatman, E. M.; Bright, V. M.; Whitesides, G. M. Surface tension-powered self-assembly of micro structures - The state-of-the-art. *J. Microelectromech. Syst.* **2003**, *12*, 387–417.
- (29) Gursoy, R. N.; Benita, S. Self-emulsifying drug delivery systems (SEDDS) for improved oral delivery of lipophilic drugs. *Biomed. Pharmacother.* **2004**, *58*, 173–182.
- (30) Kim, Y.-K.; Wang, X.; Mondkar, P.; Bukusoglu, E.; Abbott, N. L. Self-reporting and self-regulating liquid crystals. *Nature* **2018**, *557*, 539–544.
- (31) Xia, Y.; Wu, J.; Wei, W.; Du, Y.; Wan, T.; Ma, X.; An, W.; Guo, A.; Miao, C.; Yue, H.; Li, S.; Cao, X.; Su, Z.; Ma, G. Exploiting the pliability and lateral mobility of Pickering emulsion for enhanced vaccination. *Nat. Mater.* **2018**, *17*, 187–194.
- (32) Haas, P. A.; Goldstein, R. E.; Smoukov, S. K.; Cholakova, D.; Denkov, N. Theory of shape-shifting droplets. *Phys. Rev. Lett.* **2017**, *118*, 088001.
- (33) Cholakova, D.; Denkov, N.; Tcholakova, S.; Valkova, Z.; Smoukov, S. K. Multilayer formation in self-shaping emulsion droplets. *Langmuir* **2019**, *35*, 5484–5495.
- (34) Guttman, S.; Kesselman, E.; Jacob, A.; Marin, O.; Danino, D.; Deutsch, M.; Sloutskin, E.

- Nanostructures, faceting, and splitting in nanoliter to yoctoliter liquid droplets. *Nano Lett.* **2019**, *19*, 3161–3168.
- (35) Thomas, R. K.; Penfold, J. Multilayering of surfactant systems at the air-dilute aqueous solution interface. *Langmuir* **2015**, *31*, 7440–7456 .
- (36) Lidmar, J.; Mirny, L.; Nelson, D. R. Virus shapes and buckling transitions in spherical shells. *Phys. Rev. E* **2003**, *68*, 051910.
- (37) Greenfield, M. A.; Palmer, L. C.; Vernizzi, G.; de la Cruz, M. O.; Stupp, S. I. Buckled Membranes in Mixed-Valence Ionic Amphiphile Vesicles. *J. Am. Chem. Soc.* **2009**, *131*, 12030.
- (38) Dubois, M.; Deme, B.; Gulik-Krzywicki, T.; Dedieu, J.; Vautrin, C.; Desert, S.; Perez, E.; Zemb, T. Self-assembly of regular hollow icosahedra in salt-free catanionic solutions. *Nature* **2001**, *411*, 672–675.
- (39) Zwicker, D.; Seyboldt, R.; Weber, C. A.; Hyman, A. A.; Julicher, F. Growth and division of active droplets provides a model for protocells. *Nat. Phys.* **2017**, *13*, 408–413.
- (40) Cholakova, D.; Denkov, N.; Tcholakova, S.; Lesov, I.; Smoukov, S. K. Control of drop shape transformations in cooled emulsions. *Adv. Coll. Interf. Sci.* **2016**, *235*, 90 – 107.
- (41) Antl, L.; Goodwin, J. W.; Hill, R. D.; Ottewill, R. H.; Owens, S. M.; Papworth, S.; Waters, J. A. The preparation of poly(methyl methacrylate) latices in non-aqueous media. *Colloid Surface* **1986**, *17*, 67–78.
- (42) Campbell, A. I.; Bartlett, P. Fluorescent hard-sphere polymer colloids for confocal microscopy. *J. Colloid Interf. Sci.* **2002**, *256*, 325–330.
- (43) Liber, S. R.; Borohovich, S.; Butenko, A. V.; Schofield, A. B.; Sloutskin, E. Dense colloidal fluids form denser amorphous sediments. *Proc. Natl. Acad. Sci. U.S.A.* **2013**, *110*, 5769–5773.
- (44) Smith, G. N.; Ahualli, S.; Delgado, A. V.; Gillespie, D. A. J.; Kemp, R.; Peach, J.; Pegg, J. C.; Rogers, S. E.; Shebanova, O.; Smith, N.; Eastoe, J. Charging poly(methyl methacrylate)

latexes in nonpolar solvents: effect of particle concentration. *Langmuir* **2017**, *33*, 13543–13553 .

- (45) Brakke, K. A. The surface evolver. *Exp. Math.* **1992**, *1*, 141–165.
- (46) Bowick, M. J.; Giomi, L. Two-dimensional matter: order, curvature and defects. *Adv. Phys.* **2009**, *58*, 449–563.
- (47) Li, Y.; Prince, E.; Cho, S.; Salari, A.; Golestani, Y. M.; Lavrentovich, O. D.; Kumacheva, E. Periodic assembly of nanoparticle arrays in disclinations of cholesteric liquid crystals. *Proc. Natl. Acad. Sci. U.S.A.* **2017**, *114*, 2137–2142.
- (48) Fleury, J.-B.; Pires, D.; Galerne, Y. Self-connected 3D architecture of microwires. *Phys. Rev. Lett.* **2009**, *103*, 267801.
- (49) Fernández-Nieves, A.; Vitelli, V.; S, U. A.; R, L. D.; Márquez, M.; Nelson, D. R.; Weitz, D. A. Novel defect structures in nematic liquid crystal shells. *Phys. Rev. Lett.* **2007**, *99*, 157801.
- (50) Gharbi, M. A.; Seč, D.; Lopez-Leon, T.; Nobili, M.; Ravnik, M.; Žumer, S.; Blanc, C. Microparticles confined to a nematic liquid crystal shell. *Soft Matter* **2013**, *9*, 6911–6920.
- (51) DeVries, G. A.; Brunnbauer, M.; Hu, Y.; Jackson, A. M.; Long, B.; Neltner, B. T.; Uzun, O.; Wunsch, B. H.; Stellacci, F. Divalent metal nanoparticles. *Science* **2007**, *315*, 358–361.
- (52) Liu, I. B.; Sharifi-Mood, N.; Stebe, K. J. Capillary assembly of colloids: interactions on planar and curved interfaces. *Annu. Rev. Condens. Matter Phys.* **2018**, *9*, 283.
- (53) Calzolari, D. C. E.; Pontoni, D.; Deutsch, M.; Reichert, H.; Daillant, J. Nanoscale structure of surfactant-induced nanoparticle monolayers at the oil-water interface. *Soft Matter* **2012**, *8*, 11478–11483.
- (54) Binks, B. P.; Isa, L.; Tyowua, A. T. Direct measurement of contact angles of silica particles in relation to double inversion of Pickering emulsions. *Soft Matter* **2013**, *29*, 4923–4927.

- (55) Glinel, K.; Dubois, M.; Verbavatz, J.-M.; Sukhorukov, G. B.; Zemb, T. Determination of pore size of cationic icosahedral aggregates. *Langmuir* **2004**, *20*, 8546–8551.
- (56) Michina, Y.; Carrière, D.; Charpentier, T.; Brito, R.; Marques, E. F.; Douliez, J.-P.; Zemb, T. Absence of lateral phase segregation in fatty acid-based cationic mixtures. *J. Phys. Chem. B* **2010**, *114*, 1932–1938 .
- (57) Lingwood, D.; Simons, K. Lipid rafts as a membrane-organizing principle. *Science* **2010**, *327*, 46–50.
- (58) Lei, D.; Yu, Y.; Kuang, Y.-L.; Liu, J.; Krauss, R. M.; Ren, G. Single-molecule 3D imaging of human plasma intermediate-density lipoproteins reveals a polyhedral structure. *BBA - Mol. Cell Biol. L.* **2019**, *1864*, 260–270 .
- (59) Garcia-Lara, J.; Weihs, F.; Ma, X.; Walker, L.; Chaudhuri, R. R.; Kasturiarachchi, J.; Crossley, H.; Golestanian, R.; Foster, S. J. Supramolecular structure in the membrane of *Staphylococcus aureus*. *Proc. Natl. Acad. Sci. U.S.A.* **2015**, *112*, 15725–15730.

Graphical TOC Entry

